Contributed paper

PbSnTe photodiodes: theoretical predictions and experimental data

A. ROGALSKI* and R. CIUPA

Institute of Applied Physics, Military University of Technology, Warsaw, Poland

A numerical technique has been used to solve the carrier transport equations for PbSnTe photodiode configurations. The model computes the spatial distribution of the electric field, electron and hole concentrations and the generation-recombination mechanisms. Also the effect of doping profiles on the photodiode parameters (R_oA product, quantum efficiency) is analyzed. Two configurations of PbSnTe photodiodes are considered: frontside-illuminated n^+-p-p^+ PbSnTe homostructure, and double layer n-PbSeTe/p-PbSnTe backside-illuminated heterostructure. Results of calculations indicate on the potential possibilities of constructing higher quality photodiodes. The R_oA product of experimentally measured photodiodes at 77 K is controlled by Auger and Shockley-Read generation-recombination mechanisms. Theoretical predictions indicate that better performance should be received for double layer n-PbSeTe/p-PbSnTe heterostructure, which till now however have not been fabricated.

1. Introduction

For a period of one decade, from the late 1960s to the mid 1970s, because of production and storage problems, HgCdTe alloy detectors were in serious competition with ternary IV-VI alloy devices (mainly PbSnTe) for developing photodiodes [1-4]. IV-VI alloys seemed easier to prepare and appeared more stable. Development of IV-VI photodiodes was discontinued because the chalcogenides suffered two significant drawbacks. The first was a high dielectric constant that resulted in high diode capacitance and therefore limited frequency response. For scanning imaging systems under development at that time, this was a serious limitation. However, for staring imaging systems using two-dimensional arrays under development today, this would not be as significant of an issue. The second drawback of IV-VI compounds is their very high thermal coefficients of expansion [5]. This limited their applicability in hybrid configurations with silicon multiplexers. Today, with the ability to grow these materials on alternative substrates such as silicon, [6-10] this too would not be a fundamental limitation. As regards ease of manufacture, homogeneity and costs, photovoltaic IV-VI arrays on Si substrates offer substantial advantages compared to HgCdTe. The maximum available doping levels due to onset of tunnelling are more than an order of magnitude higher with IV-VIs than with HgCdTe photodiodes [3, 11, 12]. This is due to their high permittivities ε_s because tunnelling contribution of the R_oA product contains factors $\exp[\text{const}(m^*\varepsilon_s/N)^{1/2}E_g]$. The maximum allowable concentrations above 10^{17} cm^{-3} are easily controllable in IV-VIs grown by MBE.

The research group at the Swiss Federal Institute of Technology continue to pursue this technology, mainly with PbSnSe ternary alloys, and have made significant progress [6-10]. The PbSnTe photodiode technology was advancing rapidly during the early 1970s. The performance of PbSnTe photodiodes was better than HgCdTe ones at that time [13-20]. However, a little progress in the development of PbSnTe photodiode

* corresponding author: A. Rogalski, Institute of Applied Physics, Military University of Technology, 2 Kaliski Str., 01-489 Warsaw 49, Poland.

technology has been observed during last decade [21, 22].

At present, the performance of PbSnTe photodiodes is inferior to HgCdTe photodiodes, and are still below theoretical limits. Considerable improvements are possible by optimizing the device fabrication technique. Better results should be obtained using p-n junctions with a thin wider-bandgap cap layer (to reduce noise currents). This technique is successfully used in fabrication of HgCdTe photodiodes [23-32].

Theoretical performance of PbSnTe photodiodes has been determined in several papers [11, 12, 33, 34]. In these papers an one-sided abrupt junction model was assumed. Recent improvements in liquid phase epitaxy and the development of new epitaxial growth techniques (MBE and MO CVD) enables the growth of structures with very abrupt and complex doping and composition profiles which can be configured to improve device performance. These structures can not be adequately described by analytical methods and require a numerical solution.

Consequently, in the present paper a computer code to describe the behaviour of PbSnTe photodiodes is presented. The descriptions of the model, the computation technique, and results concerning quantum efficiency and R_oA product are given. Considerations concern both homojunction n^+-p-p^+ photodiode as well as heterojunction n-PbSeTe/p-PbSnTe photodiodes. Since the effect of material properties is very important in this study, a brief description of the properties of PbSnTe alloys are also given. The results of calculations are compared with experimental data. Finally, the conclusions are presented.

2. Device structures and theoretical analysis

2.1. Fundamental limitation to photodiode performance and ideal design

In this paper we will consider two configurations of PbSnTe photodiodes: frontside-illuminated n^+-p-p^+ PbSnTe homostructure, and double layer n-PbSeTe/p-PbSnTe backside-illuminated heterostructure. Homojunction structures have been most frequently used in PbSnTe photodiodes fabrication.

At first let us consider a n^+-p-p^+ PbSnTe photodiode structure shown in Fig. 1(a). We assume that the photodiode operated at 77 K is frontside -illuminated. In this type of photodiode, the base p-type layer with resultant carrier concentration of about 10^{17} cm^{-3} is sandwiched between high-doped regions. To avoid contribution of the tunneling current, the doping concentration in the base region below 10^{17} cm^{-3} is required. The thickness of the base region should be optimized for near unity quantum efficiency and a low dark current. This is achieved with a base thickness slightly higher than the inverse absorption coefficient for single pass devices: $t = 1/\alpha$ (which is ≈ 10 μm) or half of the $1/\alpha$ for double pass devices (devices supplied with a retroreflector). By thinning the base p-type region of photodiode to a thickness smaller than the minority carrier diffusion length, the corresponding R_oA product increases, provided that the device current is diffusion limited and back contact is characterized by a low recombination rate. Low doping is beneficial for a low thermal generation and a high quantum efficiency. Since the diffusion length in absorbing region is typically longer than its thickness, any carriers generated in the base region can be collected giving rise to the photocurrent. To receive high quantum efficiency, a 1-μm thick n^+-type cap layer is usually prepared with electron concentration about 10^{18} cm^{-3}. The backside p-p^+ junctions is "blocking" in nature; a more intensely doped region causes a built-in electric field that repels minority carriers, thereby reducing the recombination.

An alternative technology adopted for the preparation of LWIR PbSnTe photodiodes is the use of heterojunctions of p-type PbSnTe deposited onto n-type PbTe (PbSeTe) substrates by liquid phase epitaxy (LPE) or vapour phase epitaxy (VPE) [4]. The carrier concentration of the PbTe substrate is on the order of 10^{17} cm^{-3} which makes it transparent to photons beyond ~ 6 μm with negligible free carrier absorption ($\alpha < 5$ cm^{-1} at 10 μm) [19]. It permits complete optical utilisation of the electrical area of the photodiode, significantly reduces the optical dead-area of an array, and increases the optically sensitive area of the diode because of the refractive index mismatch between PbTe (PbSeTe) and the air. Moreover, wider energy gap material on one side of the junction results in reduction of the saturation current. Lattice mismatch between PbTe and $Pb_{1-x}Sn_xTe$ (0.4% for x = 0.2) introduces strain-relieving misfit dislocations which may be important in determining the performance of photodiodes. The lattice-matched PbSnTe/PbSeTe configuration offers a promising solution of the problem of mismatch arising in this system [20, 21].

The n-PbSeTe/p-PbSnTe heterostructure however, does not eliminate deleterious influence of ohmic contact to p-type PbSnTe layer on photodiode perfor-

mance. Better near-ideal device is double layer heterojunction (DLHJ) photodiode based on p-type material [see Fig. 1(b)]. In this case the narrow gap p-type PbSnTe base layer is sandwiched between wider gap PbSeTe regions. The wider bandgap cap region contributes a negligible amount to the thermally generated diffusion current compared with that from the p-type PbSnTe absorbing layer. Also deleterious effect of ohmic contacts on device performance is suppressed. It should be noticed that the proposed DLHJ PbSnTe photodiode has not been realized in practice.

2.2. Method of calculation

For simplicity, we take the one-dimensional model for the photodiode. We assume that the uniform signal photon flux ϕ_s is incident on the photodiode area A. The influence of assuming doping profile on photodiode performance has been solved by forward-condition steady-state analysis [35]. Basic equations for d.c. analysis include the well known equations: two current density equations for electrons and holes, two continuity equations for electrons and holes and Poisson's equation which are collectively referred to as the Van Roosbroeck model [36].

In order to execute a dc steady-state numerical analysis the equations were transformed into difference equations in which the variables were defined at a finite number of division points. The meshpoint spacing was defined as a function of the space co-ordinate x. The choice of fine spacing for a high-field depletion layer and a coarse spacing for a neutral region was preferable. Practically, the meshpoint spacing from 5×10^{-8} m to 2×10^{-7} m had been used. The quantities of current density, generation and recombination rates are non-linear functions and they are linearized by the Taylor expansion regarding fundamental variables p, n and the electric potential, with neglecting of higher-order terms. The solution of original differential equations is then replaced by that of the matrix vector equation. The method can be related to as the iteration Newton procedure. More exact description of this type of calculations can be found in Kurata's monographs [35]. This method of numerical calculations has been recently used in our papers [37, 38].

In the case of ohmic contacts, the carrier concentrations at the contacts are equal to their equilibrium values. This implies infinite rate of generation and recombination at the surfaces. Therefore, e.g., the boundary condition for ohmic contact at the front surface is

$$p(0) = p_o(0) \tag{1}$$

The generation-recombination term (G–R) [which occurs in the continuity equations] is associated with the predominant recombination mechanisms. There are three important carrier generation and recombination mechanisms: Shockley-Read (SR), radiative, and Auger mechanisms. The SR mechanism occurs via lattice defect and impurity energy levels within the forbidden energy gap. This mechanism can be controlled by the procedure used to grow the material; consequently, SR process is not a fundamental limit to the performance of the detectors.

The role of radiative mechanism in detection of IR radiation has been critically reexamined by Humpreys [39, 40]. He indicated that most photons emitted in detectors are immediately re-absorbed as a result of radiative decay, so that the observed radiative lifetime is only a measure of how well photons can escape from the body of detector. Due to re-absorption the radiative lifetime is highly extended, depending on the device geometry. The calculations which are often used in the literature to model the performance of detectors are based on incorrectly derived recombination lifetime using the Van Roosbroeck and Shockley theory [41]. This leads to an underestimated detectivity. Since the reabsorption conditions are specified for each real case, and in general are not exactly known, in the present paper the (G–R) term for radiative process is calculated in the traditional manner.

A consequence of the similar valence and conduction bands of lead salts is that the electron and hole mobilities are approximately equal for the same temperatures and doping concentrations. In high-quality PbSnTe single crystals for temperature range above 77 K, the mobility varies as $T^{-2.5}$ [42, 43]. This behaviour has been ascribed to a combination of polar-optical and acoustical lattice vibrations. For PbSnTe alloy we assume that $\mu_{e,h} = 10^9 T^{-2.5}$ cm^2/Vs.

The net recombination rate due to SR states is given by [44]

$$(R\text{–}G)_{SRH} = \left[n(x)p(x) - n_i^2\right]\left[\tau_{po}\left(n(x) + n_i \exp\frac{E_t - E_i}{kT}\right) + \tau_{no}\left(p(x) + n_i \exp\frac{E_i - E_t}{kT}\right)\right]^{-1} \tag{2}$$

where τ_{no} and τ_{po} are the low-level minority carrier lifetimes due to SR process, E_t is the trap energy level, n_i is the intrinsic carrier density and E_i is the intrinsic

Fermi level. Obviously in thermal equilibrium, $np = n_i^2$ and the net recombination rate is equal to zero. Through-out this calculation a midband-gap trap level is assumed.

The intrinsic carrier concentration in $Pb_{1-x}Sn_xTe$ can be calculated according to the expression [45]

$$n_i = \left(8.92 - 34.46x + - 2.55 \times 10^{-3}T + 4.12 \times 10^{-2}xT + 97.00x^2\right) \times 10^{14} E_g^{3/2} \exp\left(-\frac{E_g}{2kT}\right) \quad (3)$$

The net recombination rate due to the radiative process is [46]

$$(R - G)_R = G_R\left[n(x)p(x) - n_i^2\right] \quad (4)$$

In terms of the Kane-type two-band model [47]

$$G_R = \frac{2n_r q^2 (2P_t^2 + P_l^2) E_g^4}{9\varepsilon_o h^4 c^3 P_t^2 P_l \pi^3} F(\beta) \quad (5)$$

where

$$\Phi(t) = t^{1/2}\left(1 + \frac{t}{\beta}\right)^{1/2}\left(3 + \frac{8t}{\beta} + \frac{8t^2}{\beta^2}\right)$$

$$t = \frac{\beta(z-1)}{2}, \quad z = \frac{h\nu}{E_g}, \quad \beta = \frac{E_g}{kT}$$

$$n_o + p_o = 2\left(\frac{N_d^2}{4} + n_i^2\right)^{1/2}$$

In the above equations n_r is the refraction coefficient, ε_r is the static dielectric constant, h is the Planck constant, c is the speed of light, q is the electron charge, k is the Boltzman's constant, and P_t and P_l are the transverse and longitudinal momentum matrix elements.

For lead salts, the valence band and the conduction band with mirror-reflection symmetry occur at point L of the Brillouin zone (number of valleys N = 4). In such a case the energy and momentum conservation laws are difficult to fulfil for impact recombination, especially for carriers near the band edges when only single-valley interaction is taken into account. Two types of Auger process should be considered:
(a) all scattered carriers are at a definite point of the Brillouin zone;
(b) the initial carriers are in different valleys at the band.

The Auger process in small-gap IV-VI semiconductors is not fully clarified [48]. Discrepancy concerns both experimental as well as theoretical results. Disagreement between theoretical papers are due to the lack of accurate band parameters for lead salts and to the theoretical description of screening in the Auger process. Considerations carried out by Emtage indicate that in PbSnTe alloys the inter-valley interaction is a more efficient channel of Auger recombination than scattering within a single ellipsoid. According to the intervalley carrier interaction model an electron and hole from one valley (characterized by "heavy" mass m_l^*) and a third carrier from another valley with a "light" mass m_t^*, participate in impact recombination in the given direction. As a result of this interaction the "heavy" electron and hole carrier recombine and the liberated energy and momentum are transferred to the "light" carrier.

The net recombination rate due to Auger process is given by

$$(R - G)_A = G_A\left[n^2(x)p(x) - n_o^2 p_o\right] \quad (6)$$

For intervalley process proposed by Emtage [49]

$$G_A = (2\pi)^{5/2} \frac{N-1}{N^2} \frac{q^4}{(4\pi\varepsilon_o\varepsilon_\infty)^2} (kT)^{1/2} E_g^{-7/2} \frac{\hbar^3}{m_l^{*1/2} m_t^{*3/2}} \exp\left[-\frac{E_g K^{-1}}{2kT}\right] \quad (7)$$

where $K = m_l^*/m_t^* = P_t^2/P_l^2$ is the effective mass anisotropy coefficient. The values of longitudinal m_l^* and transverse mass m_t^* components can be found from relations:

$$m_t^* = \frac{\hbar^2 E_g}{2P_t^2} \quad \text{and} \quad m_l^* = \frac{\hbar^2 E_g}{2P_l^2} \quad (8)$$

The Emtage expression includes non-degeneration statistics, nevertheless it is a good approximation of more precisely calculated Auger coefficients [50].

The basic material parameters of PbSnTe assumed in calculations are listed in Table 1.

Table 1. Band structure parameters of $Pb_{1-x}Sn_xTe$ assumed in calculations [3, 51].

E_g (meV)	$171 - 535x + (400 + 0.256T^2)^{1/2}$
$P_l^*(10^{-8}$ eVcm)	1.4
$P_t^*(10^{-8}$ eVcm)	4.6
n_r	$(300/E_g)^{1/4}$
ε_∞	$(300/E_g)^{1/2}$

The position dependent optical generation rate $G_o(x)$ can be calculated as

$$G_o(x) = \frac{P_o(1-r)}{A}\frac{\lambda e^{-\alpha x}}{hc} \tag{9}$$

where P_o is the radiation power, A is the detector area, and r is the surface reflection coefficient equal to 0.5. The absorption coefficient has been calculated according to Anderson expression [52] delivered within the Kane model and taking into account the Burstein-Moss bandfiling effect.

The magnitude of the quantum efficiency can be determined from the relations

$$\eta = \frac{I_{ph}}{q\Phi_s} \tag{10}$$

where I_{ph} is the photocurrent, and Φ_s is the incident photon flux connected with the radiation power by the relation $P_o = (hc/\lambda)\Phi_s$.

To calculate the local photoelectric gain in a given small segment Δx_i of the photodiode, we are using following procedure. At first we assume an additional generation of charge carriers in this segment ΔG_i and then we solve the set of Van Roosbroeck's equations with and without the additional generation. The photoelectric gain is then calculated as

$$g_i = \frac{\Delta I_i}{q\Delta G_i \Delta x_i} \tag{11}$$

where ΔI_i is the change of current density due to increased generation in the segment Δx_i.

The current passing contacts of the device is noisy due to statistical nature of generation and recombination processes. Assuming that the current gains for photocurrent and noise current are the same, the current noise is equal to [53]

$$I_{fi}^2 = \int_0^t 2q^2(G+R)A_e g^2 \Delta f dx \tag{12}$$

where t is the detector thickness, A_e is the electrical area of the detector, and Δf is the electrical bandwidth of the receiver.

It should be noted that the effects of fluctuating recombination rate can be frequently avoided by arranging for the recombination process to take place in a region of the device where it has little effect due to low photoelectric gain; for example, at the contacts in sweep-out photoconductors or in the neutral regions of the diodes. The generation process with its associated fluctuation, however, cannot be avoided by any means.

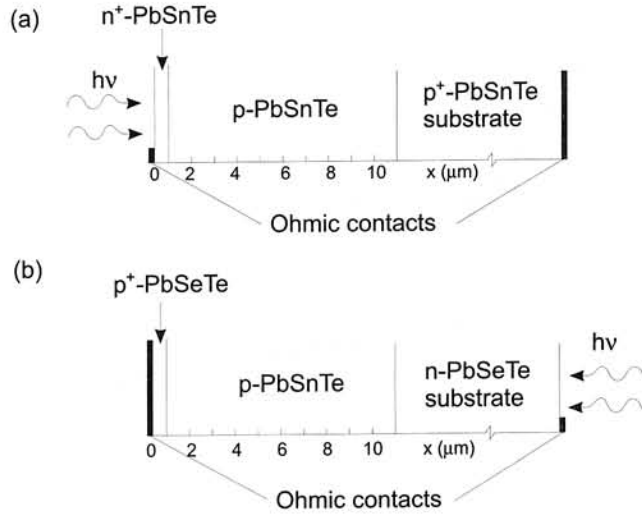

Fig. 1. Schematic drawing of: (a) n^+-p-p^+ PbSnTe homojunction structure; (b) DLHJ PbSnTe structure.

3. Results and discussion

The profile of the equilibrium concentrations ("n_o" and "p_o") and the electric field E(x) across n^+-p-p^+ $Pb_{0.783}Sn_{0.217}Te$ photodiode at 77 K (E_g = 0.1 eV), in the absence of bias voltage and IR flux, is shown in

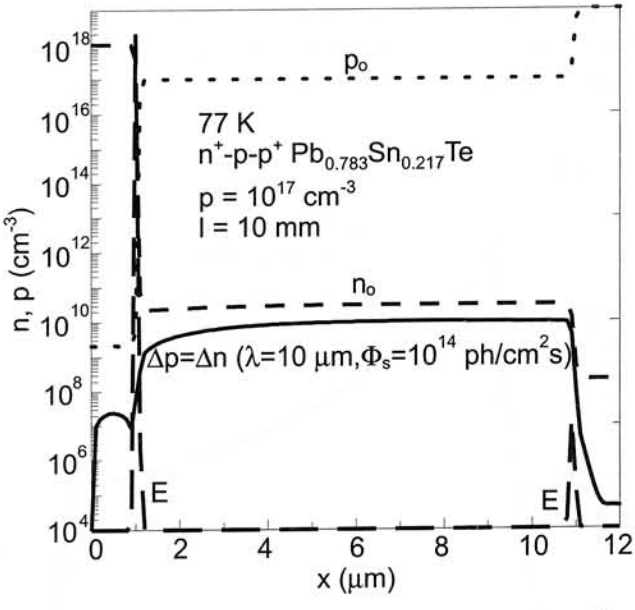

Fig. 2. Equilibrium and excess carriers concentration profiles and electric fields across n^+-p-p^+ $Pb_{0.783}Sn_{0.217}Te$ homojunction at 77 K in the absence of bias voltage. The excess carrier concentration profiles is calculated in the presence of an infrared flux 10^{14} photons/cm^{2}s at λ = 10 μm.

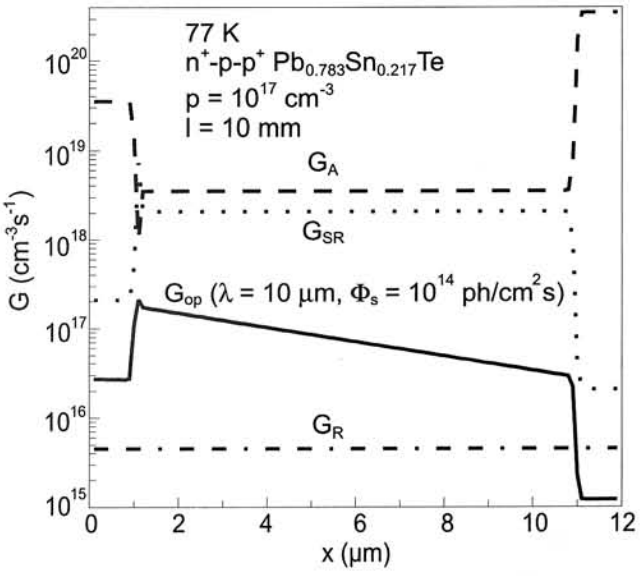

Fig. 3. The radiative, Auger and SR generation vs position for across n^+-p-p^+ $Pb_{0.783}Sn_{0.217}Te$ photodiode at 77 K in the absence of bias voltage. Optical generation rate is calculated assuming incident photon flux of 10^{14} photons/cm^{2}s at λ = 10 μm.

Fig. 2. As expected, the electric field is associated with the n^+-p junction. Also the characteristic of the back-side field of the p-p^+ junction is also apparent in the profile.

The photonic behaviour of the photodiode can easily be examined by introducing an incident photon flux. We can see from Fig. 2 that in the presence of infrared flux, concentration of both majority and minority carriers increases, what is shown by $\Delta n = \Delta p$ curve. In addition, it should be noticed, that in the proximity of n^+-p homojunction the carriers are extracted by electric field of junction. This effect is easily observed for minority carriers (since $n_o << p_o$ and $\Delta n = \Delta p << p_o$) and can be intensified under reverse bias of photodiode.

Fig. 3 shows the radiative, Auger and SR generation rates, and the optical generation rate created by incident flux in n^+-p-p^+ $Pb_{0.783}Sn_{0.217}Te$ homojunction. In calculations of SR generation the value of $\tau_{no} = \tau_{po} = 10^{-8}$ s was assumed. Because of the higher doping level of the front surface (n^+), the Auger mechanism is clearly dominant here. In the depletion region of n^+-p junction, SR generation is enhanced, instead in the central p-type region with $N_a = 10^{17}$ cm^{-3} contributions of Auger mechanism and SR mechanism are comparable. Influence of SR mechanism can be diminished using better quality p-type material with higher values of τ_{no} and τ_{po}. The optical generation decreases toward the backside surface since the device is frontside-illuminated.

Figure 4 presents the distribution of the local photoelectric gain across the thickness of n^+-p-p^+ $Pb_{0.783}Sn_{0.217}Te$ photodiode at 77 K. We can see that near p-n junction the photogain is equal 1 and decreases as the distance from the junction increases. Distribution of the photogain indicates that the minority carrier diffusion length L_e is comparable with the thickness of base p-type layer of photodiode. L_e estimated from the equation $L_e = [(kT/q)\mu_e\tau_e]^{1/2}$ is equal to 12 μm. To improve distribution of the photogain, L_e should be much larger thickness than that of p-type base layer (in our consideration equal 10 μm). It is partly possible using better quality p-type material with lower density of SR recombination centres.

The value of $(G+R)g^2$ reflects the distribution of the generation-recombination noise power density [see Eq. (12)] across the diode, which is shown in Fig. 5. The main contribution to the total noise (measured as an area below solid line in Fig. 5) comes from the p-type base region. Due to high electron concentration, the maximum value of noise power density is achieved in n^+-region. However, contribution from this region to the total noise of the photodiode is insignificant, since the n^+-region is narrow. Contributions from both n^+- and n^--regions to the total noise of the photodiode can be suppressed by using wider band gap energy n-type cap layer and electrical junction positioned near metallurgical interface in the small gap p-type base layer.

The dependence of the internal quantum efficiency on the dopant concentrations in central p-type base region for n^+-p-p^+ $Pb_{0.783}Sn_{0.217}Te$ photodiode at 77 K

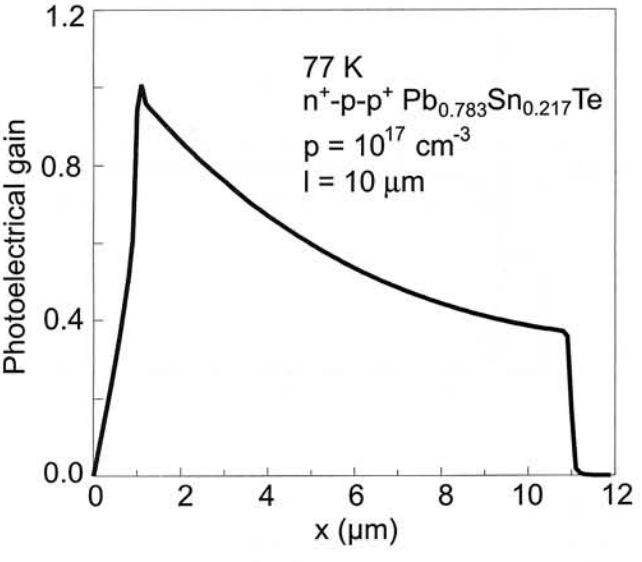

Fig. 4. Distribution of the photoelectrical gain across n^+-p-p^+ $Pb_{0.783}Sn_{0.217}Te$ photodiode at zero bias voltage and at 77 K.

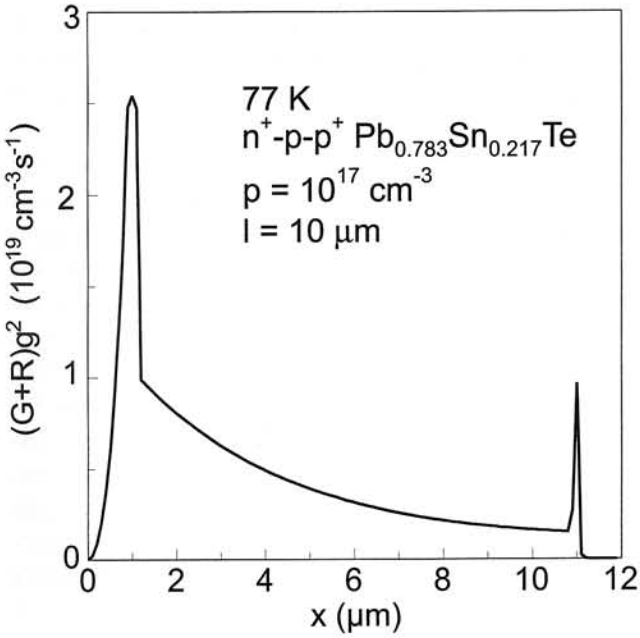

Fig. 5. Distribution of $(G+R)g^2$ factor across across n^+-p-p^+ $Pb_{0.783}Sn_{0.217}Te$ photodiode at zero bias voltage and at 77 K.

is shown in Fig. 6. We can see that at dopant concentration 10^{17} cm^{-3} a sufficiently high internal quantum efficiency of about 70% is attainable. However, Fig. 6 indicates that at acceptor concentration above 1017 cm^{-3} the quantum efficiency considerably decreases due to the influence of Burstein-Moss effect. It should be

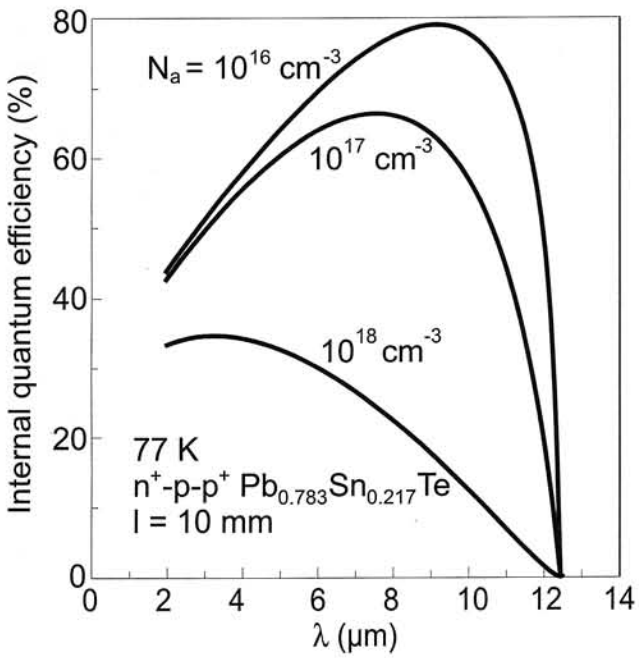

Fig. 6. The dependence of the internal quantum efficiency on acceptor concentration in p-type base region of across n^+-p-p^+ $Pb_{0.783}Sn_{0.217}Te$ at 77 K.

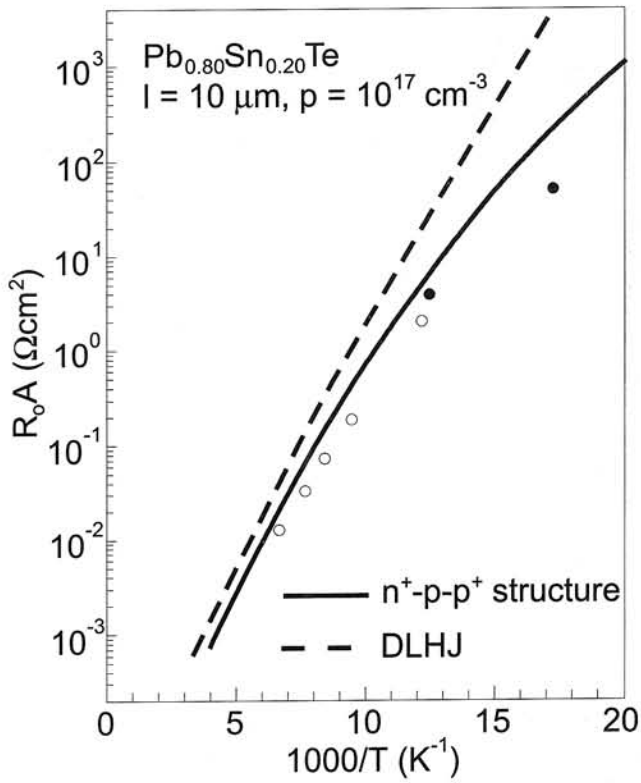

Fig. 7. Temperature dependence of the R_oA product of $Pb_{0.80}Sn_{0.20}Te$ photodiode. The experimental data are taken from Refs: 13 (o) and 22 (•). The solid line is calculated for n^+-p-p^+ $Pb_{0.80}Sn_{0.20}Te$ homojunction photodiode, instead the dashed line is calculated for DLHJ $Pb_{0.80}Sn_{0.20}Te$ photodiode structure shown in Fig. 1(b).

noticed that without antireflection coating the surface reflection coefficient is about 0.5.

In Fig. 7, the R_oA product versus temperature is presented under a 0° FOV for $Pb_{0.80}Sb_{0.20}Te$ photodiode with cutoff wavelength of 11.8 μm at 77 K. Good agreement between experimental data (taken from papers of another authors) and theoretical calculations (solid line) has been achieved. It should be noticed however, that for more optimized DLHJ structure, theoretically predicted values of the R_oA product are higher (see dashed line). The increase of R_oA product for DLHJ photodiodes will be more emphasized in the case of higher quality p-type base PbSnTe layer, when contribution of Shockley-Read generation will be suppressed (for higher values of τ_{no} and τ_{po}; in our calculations we assumed $\tau_{no} = \tau_{po} = 10^{-8}$ s). It should be noticed however, that due to inherently higher Auger generation rate in PbSnTe in comparison with HgCdTe, the enhancement of R_oA product of PbSnTe photodiodes is more limited in comparison with HgCdTe photodiodes [4, 54].

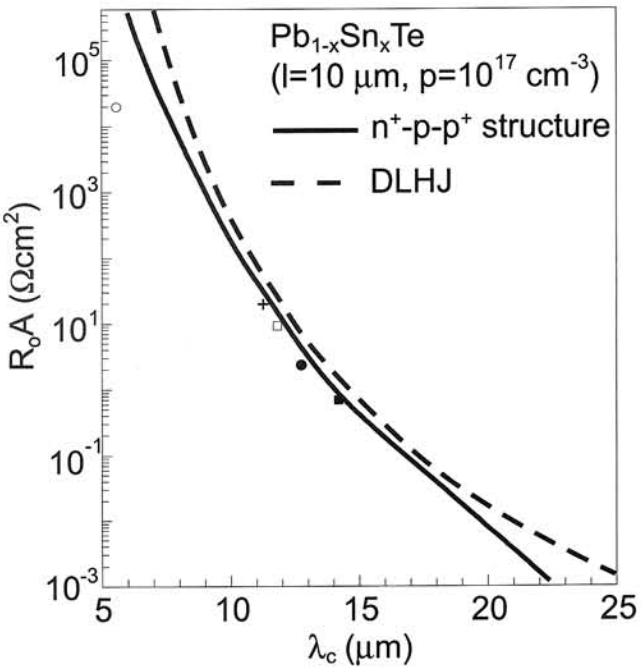

Fig. 8. Dependence of the R_oA product on the long wavelength cutoff for PbSnTe photodiodes at 77 K. The experimental data are taken from Refs: 13 (+), 14 (•), 15, 17 (❑), 18 (o), and 20 (■). The solid line is calculated for n^+-p-p^+ PbSnTe homojunction photodiodes, instead the dashed line is calculated for DLHJ PbSnTe photodiode structures shown in Fig. 1(b).

The last figure (Fig. 8) shows the dependence of the R_oA product on the long wavelength cutoff for LWIR PbSnTe photodiodes at 77 K. In this figure a selection of experimental data are also observed. A satisfactory agreement between the theoretical curves and the experimental data has been achieved for n^+-p-p^+ homojunction structures. In the short wavelength region the discrepancy between the theoretical curve and experimental data increases, which is due to additional currents in the junctions (such as the generation-recombination current of the depletion region or the surface leakage current) that are not considered. Theoretically calculated curve for DLHJ structures is situated above experimentally measured values of the R_oA product, what indicate the potential possibilities of constructing higher quality PbSnTe photodiodes.

4. Conclusions

In this paper the performance of LWIR PbSnTe photodiodes is analyzed. The effect of doping profile on the photodiode parameters (R_oA product, quantum efficiency and noise) is solved by forward-condition steady-state analysis. The model computes the spatial distribution of the electric potential, electric field, electron and hole concentrations and the generation-recombination mechanisms. This model is also used to give insight into the forces controlling charge carrier motion, the mechanisms controlling charge carrier generation or loss, and the effect that these phenomena have on the performance of photodiode. Good agreement between experimental data and theoretical calculations of the R_oA product has been achieved for n^+-p-p^+ PbSnTe homojunction photodiodes. The R_oA product of experimentally measured n^+-p-p^+ PbSnTe photodiodes at 77 K is controlled by Auger and SR generation-recombination mechanisms. Results of calculations indicate on potential possibilities of constructing higher quality PbSnTe photodiodes, especially using double layer n-PbSeTe/p-PbSnTe heterostructures. Up to now however, this type of PbSnTe photodiode structure has not been fabricated.

References

1. I. Melngailis and T. C. Herman: in *Semiconductors and Semimetals*, Vol. 5, p. 111, ed. R.K. Willardson and A. C. Berr, (Academic Press, New York, 1970).
2. T. C. Herman and I. Melngailis: in *Applied Solid-State Science*, Vol. 4, p. 1, R. Wolfe (Academic Press, 1974).
3. A. Rogalski and J. Piotrowski: *Prog. Quant. Electron.* **12** (1988) 87.
4. A. Rogalski: in *Infrared Photon Detectors* p. 513, SPIE Optical Engineering Press, (Bellingham, 1995).
5. J. T. Longo, D. T. Cheung, A. M. Andrews, C. C. Wang and J. M. Tracy: *IEEE Trans. Electron Devices* **ED-25** (1978) 213.
6. H. Zogg, S. Blunier, T. Hoshino, C. Maissen, J. Masek and A. N. Tiwari: *IEEE Trans. Electron Devices* **ED-38** (1991) 1110.
7. H. Zogg, C. Maissen, J. Masek, T. Hoshino, S. Blunier and A. N. Tiwari: *Semicon. Sci. Technol.* **6** (1991) C36.
8. T. Hoshino, C. Maissen, H. Zogg, J. Masek, S. Blunier, A. N. Tiwari, S. Teodoropol and W. J. Bober: *Infrared Phys.* **32** (1991) 169.
9. J. Masek, T. Hoshino, C. Maissen, H. Zogg and S. Blunier: *Proc. SPIE* **1735** (1992) 54.
10. H. Zogg, A. Fach, J. John, J. Masek, P. MĆller, C. Paglino, and W. Buttler: *Proc. SPIE* **2552** (1995).
11. H. Preier: *Infrared Phys.* **18** (1979) 43.
12. A. Rogalski and W. Larkowski: *Electron Technology* **18** (3/4) (1985) 55.

13. C. A. Kennedy, K. J. Linden and D. A. Soderman: *Proc. IEEE* **63** (1975) 27.
14. C. C. Wang and S. R. Hampton: *Solid-State Electronics* **18** (1975) 121.
15. P. S. Chia, J. R. Balon, A. H. Lockwood, D. M. Randall, F. J. Renda, L. H. DeVaux and H. Kimura: *Infrared Phys.* **15** (1975) 279.
16. M. R. Johnson, R. A. Chapman, and J. S. Wrobel: *Infrared Phys.* **15** (1975) 317.
17. C. C. Wang and J. S. Lorenzo: *Infrared Phys.* **17** (1977) 83.
18. C. H. Gooch, H. A. Tarry, R. C. Bottomley, M. G. Astles and B. J. Waldock: *Electronics Lett.* **14** (1978) 209.
19. C. C. Wang, M. H. Kalisher, J. M. Tracy, J. E. Clarke and J. T. Longo: *Solid-State Electronics* **21** (1978) 625.
20. C. C. Wang and M. E. Kim: *J. Appl. Phys.* **50** (1979) 3733.
21. V. V. Tetyorkin, V. B. Alenberg, F. F. Sizov, E. V. Susov, Yu. G. Troyan, A. V. Gusarov, V. Yu. Chopik and K. S. Medvedev: *Infrared Phys.* **30** (1990) 499.
22. V. F. Chishko, V. T. Hryapov, I. L. Kasatkin, V. V. Osipov and O. V. Smolin: *Infrared Phys.* **33** (1992) 275.
23. G. N. Pultz, P. W. Norton, E. E. Krueger and M.B. Reine: *J. Vac. Sci. Technol.* **B9** (1991) 1724.
24. C. C. Wang: *J. Vac. Sci. Technol.* **B9** (1991) 1740.
25. R. E. DeWames, J. M. Arias, L. J. Kozlowski, and G. M. Williams: *Proc. SPIE* **1735** (1992) 3.
26. T. Tung, L. V. DeArmond, R. F. Herald, P. E. Herning, M. H. Kalisher, D. A. Olson, R. F. Risser, A. P. Stevens and S. J. Tighe: *Proc. SPIE* **1735** (1992) 109.
27. J. M. Arias, J. G. Pasko, M. Zandian, S. H. Shin, G. M. Williams, L. O. Bubulac, R. E. DeWames and W. E. Tennat: *Appl. Phys. Lett.* **62** (1993) 976.
28. S. M. Johnson, J. A. Vigil, J. B. James, C. A. Cockrum, W. H. Konkel, M. H. Kalisher, R. F. Risser, T. Tung, W. J. Hamilton, W. L. Ahlgren, and J. M. Myrosznyk: *J. Electron. Mat.* **22** (1993) 835.
29. M. B. Reine, K. R. Maschhoff, S. P. Tobin, P. W. Norton, J. A. Mroczkowski, and E. E. Krueger: *Semicon. Sci. Technol.* **8** (1993) 788.
30. J. M. Arias, J. G. Pasko, M. Zandian, L. J. Kozlowski, and R. E. DeWames: *Opt. Eng.* **33** (1994) 1422.
31. T. J. de Lyon, S. M. Johnson, C. A. Cockrum, O.K.Wu, W. J. Hamilton and G. S. Kamath: *J. Electrochem. Soc.* **141** (1994) 2888.
32. J. Piotrowski, in *Infrared Photon Detectors,* p. 391, edited by A. Rogalski: SPIE Optical Engineering Press, (Bellingham, !995).
33. M. Grudzieé and A. Rogalski: *Infrared Phys.* **21** (1981) 1.
34. A. Rogalski and J. Rutkowski: *Infrared Phys.* **21** (1981) 191.
35. M. Kurata: *Numerical Analysis of Semiconductor Devices,* Lexington Books, 1982.
36. W. Van Roosbroeck: *Bell Syst. Tech. J.* **29** (1950) 560.
37. A. Rogalski, Ciupa and H. Zogg: *Infrared Phys. Technol.* **35** (1994) 837.
38. A. Rogalski and R. Ciupa: *J. Appl. Phys.* **77** (1995) 3505.
39. R. G. Humpreys: *Infrared Phys.* **23** (1983) 171.
40. R. G. Humpreys: *Infrared Phys.* **26** (1986) 337.
41. W. Van Roosbroeck and W. Shockley: *Phys. Rev.* **94** (1954) 1558.
42. Yu. I. Ravich, B. A. Effimova and I. A. Smirnov: *Semiconducting Lead Chalcogenides,* Plenum, New York (1970).
43. R. Dornhaus, G. Nimtz and B. Schlicht: *Narrow-Gap Semiconductors,* (Springer, Berlin 1985).
44. S.M. Sze: *Physics of Semiconductor Devices*, Wiley, New York (1981).
45. A. Rogalski and K. Jóźwikowski: *Phys. Stat. Sol.* **A111** (1989) 559.
46. R. N. Hall: *Proc. IEE* **B 106** (Suppl. 17) (1959) 923.
47. O. Ziep, D. Genzow, M. Mocker and K. H. Herrmann: *Phys. Stat. Sol. (b)* **99** (1980) 129.
48. A. Rogalski: in *Infrared Photon Detectors,* p. 145, SPIE Optical Engineering Press, Bellingham (1995).
49. P. R. Emtage: *J. Appl. Phys.* **47** (1976) 2565.
50. M. S. Adler, C. R. Hewes and S. D. Senturia: *Phys. Rev.* **B7** (1973) 5186.
51. O. Ziep, M. Mocker: *Phys. Stat. Sol.* **B98** (1980) 133.
52. W. W. Anderson: *Infrared Phys.* **20** (1980) 363.
53. A. Rose: *Concepts in Photoconductivity and Allied Problems,* (Interscience Publishers, New York, 1963).
54. A. Rogalski and R. Ciupa: *J. Appl. Phys.,* to be published.